

Temperature and doping dependencies of electrical properties in Al-doped 4H-SiC epitaxial layers

Atsushi Koizumi,^{a)} Jun Suda, and Tsunenobu Kimoto

Department of Electronic Science and Engineering, Kyoto University, Kyotodaigaku-katsura, Nishikyo, Kyoto 615-8510, Japan

(Received 26 November 2008; accepted 31 May 2009; published online 13 July 2009)

The free hole concentration and the low-field transport properties of Al-doped 4H-SiC epilayers with several acceptor concentrations grown on semi-insulating substrates have been investigated in the temperature range from 100 to 500 K by Hall-effect measurements. Samples have been grown by cold-wall chemical vapor deposition (CVD) in the Al acceptor concentration range from 3×10^{15} to 5.5×10^{19} cm⁻³. The dependencies of the acceptor ionization ratio at 300 K and the ionization energy on the acceptor concentration were estimated. Numerical calculations of the hole Hall mobility and the Hall scattering factor have been performed based on the low-field transport model using relaxation-time approximation. At the low acceptor concentrations, the acoustic phonon scattering dominates the hole mobility at 300 K. At the high acceptor concentrations, on the other hand, the neutral impurity scattering dominates the mobility. A Caughey–Thomas mobility model with temperature dependent parameters is used to describe the dependence of the hole mobilities on the acceptor concentration, and the physical meanings of the parameters are discussed. © 2009 American Institute of Physics. [DOI: [10.1063/1.3158565](https://doi.org/10.1063/1.3158565)]

I. INTRODUCTION

Silicon carbide (SiC) is an attractive wide bandgap semiconductor material for use in high-power, high-frequency, and high-temperature device applications, since it has superior physical and electronic properties such as high breakdown field, high thermal conductivity, and high saturation electron drift velocity.^{1,2} Among a number of SiC polytypes, 4H-SiC is a key material for manufacturing electronic devices because of a wider bandgap, high electron mobility, and its small anisotropy.

For characterizing the transport of charged carriers and formulating the current in semiconductor devices, it is important to understand a full picture of transport properties such as the dependence of the carrier concentrations and the mobilities in SiC on temperature and doping concentration in both the *n*- and *p*-type materials since SiC devices operate in a wide temperature range. A great deal of attention has been paid to the electron transport properties in SiC,^{3–5} but for the *p*-type 4H-SiC, there have been only a few reports on the fundamental properties such as the acceptor-concentration dependence of the ionization energy and the temperature dependence of the hole mobility.^{6–8}

Aluminum (Al) has been particularly attractive to form heavily doped *p*⁺-regions with reasonable sheet resistance because Al acceptors have smaller ionization energy (191–230 meV) (Refs. 9 and 10) than boron (B) acceptors (285–390 meV) (Refs. 11 and 12) in 4H-SiC.

In this study, the authors have investigated fundamental electrical properties of Al-doped 4H-SiC such as ionization energy and mobility by Hall-effect measurements. To clarify the hole scattering mechanisms, the authors calculated the temperature dependence of the hole mobility considering the

neutral impurity scattering, the ionized impurity scattering, and the lattice scatterings, and the major scattering mechanism is discussed.

II. EXPERIMENTAL DETAILS

A series of Al-doped 4H-SiC samples with different Al doping concentrations were grown by atmospheric-pressure chemical vapor deposition (CVD) with a horizontal cold-wall reactor in a SiH₄–C₃H₈–H₂ system.¹³ The samples were grown on commercially available high-purity semi-insulating 4H-SiC (0001) wafers 8° off-oriented toward $\langle 11\bar{2}0 \rangle$. The samples were etched by HCl [3 SCCM (SCCM denotes cubic centimeter per minute at STP)] with H₂ carrier gas (1.0 slm) at 1300 °C for 20 min in the CVD reactor. After the HCl/H₂ etching, the substrate temperature was increased to 1500 °C, and the epitaxial growth was started. *In situ* Al doping was performed by simultaneous supply of trimethylaluminum (TMAI) during growth with a constant C/Si ratio of 3. The flow rates of SiH₄, C₃H₈, and H₂ were 0.50 SCCM, 0.50 SCCM, and 3.0 slm, respectively, which resulted in a growth rate of 3.3 μm/h. The thicknesses of the Al-doped epilayers were 5.5–6.6 μm. The variation of the thickness comes from different growth time, which was intentionally changed. The TMAI flow rate was varied in the range from 1.5×10^{-3} to 3.0×10^{-1} SCCM. For the samples grown under the conditions of TMAI flow rate lower than 1.5×10^{-2} SCCM, the TMAI vapor diluted to 150 ppm in H₂ gas was used. For the higher TMAI flow rate conditions, the TMAI vapor was generated by bubbling H₂ as a carrier gas. The TMAI source temperature was kept at 17 °C. All samples have a smooth surface with no evidence of step bunching determined by atomic force microscope.

After the growth, ion implantation of Al⁺ was carried out for the lightly doped samples to obtain low-resistance Ohmic

^{a)}Electronic mail: koizumi@semicon.kuee.kyoto-u.ac.jp.

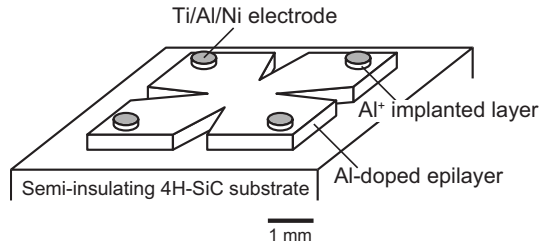


FIG. 1. The schematic structure of the sample for Hall-effect measurements.

contacts, especially at low temperature. The postimplantation annealing was performed in the CVD reactor at 1550 °C for 20 min in the atmospheric pure Ar ambience. For Ohmic contacts, Ti/Al/Ni was evaporated on the surface through a mask followed by rapid thermal annealing at 1000 °C in Ar ambience for 10 min. The clover-leaf-shaped mesa structure was fabricated by reactive ion etching (RIE) for Hall-effect measurements. The Al⁺-implanted layer near the surface except for the region beneath the electrodes was removed by RIE using the electrode metal as an etching mask. The schematic structure of the sample is shown in Fig. 1. Variable-temperature Hall-effect measurements using van der Pauw configuration were performed in a temperature range from 100 to 500 K and in a magnetic field of 0.5 T using a Hall measurement system (HL5500) from Accent Optical Technologies.

III. RESULTS AND DISCUSSION

A. Temperature dependence of hole concentration

Figure 2 shows the temperature dependence of the free hole concentration p for the Al-doped 4H-SiC epilayers with different acceptor concentrations. The free hole concentrations are determined from the measured Hall constant R_H using

$$p = \frac{r_H}{qR_H}, \quad (1)$$

where r_H is the Hall scattering factor for holes, assumed to be unity independent of temperature in this figure, and q is

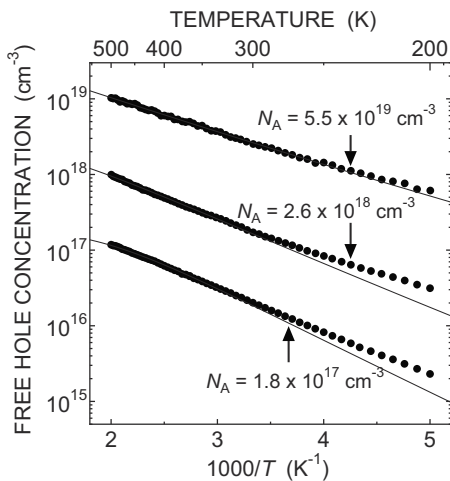


FIG. 2. Temperature dependence of free hole concentration for Al-doped 4H-SiC with different acceptor concentrations.

the elementary charge. The hole concentrations were exponentially increased with increasing temperature. The acceptor concentration was evaluated by a least squares fit of the neutrality equation based on the Boltzmann approximation with a single acceptor level to the experimental data. The neutrality equation is given by

$$p + N_{\text{comp}} = \frac{N_A}{1 + \frac{g(T)p}{N_V(T)} \exp\left(\frac{\Delta E_A}{k_B T}\right)}, \quad (2)$$

where N_A is the concentration of acceptors, ΔE_A the ionization energy of Al acceptor, N_{comp} the concentration of compensating states, $g(T)$ the temperature dependent acceptor degeneracy factor, T the absolute temperature, and k_B the Boltzmann constant. The effective density of states $N_V(T)$ in the valence band is given by

$$N_V(T) = 2 \left[\frac{2\pi m_{\text{dh}}^*(T) k_B T}{h^2} \right]^{3/2}, \quad (3)$$

where h is the Planck constant and $m_{\text{dh}}^*(T)$ is the temperature dependent density-of-state effective mass of hole in 4H-SiC, which is calculated by Wellenhofer *et al.*¹⁴

The temperature dependence of $g(T)$ comes from possible excited ground states of the aluminum acceptor.^{8,15} Recently, Matsuura *et al.* proposed a distribution function, which was considered an ensemble average $\overline{E_{\text{ex},n}(T)}$ of the ground and excited state levels of the acceptor into the distribution function in addition to the excited states.¹⁶⁻¹⁸ In the distribution function, the degeneracy factor $g_n(T)$ is given by¹⁶

$$g_n(T) = g_A \exp\left(-\frac{\overline{E_{\text{ex},n}(T)}}{k_B T}\right) \times \left[1 + \sum_{r=2}^n g_r \exp\left(\frac{\Delta E_r - \Delta E_A}{k_B T}\right) \right], \quad (4)$$

where ΔE_r is the energy separation between E_V and the $(r-1)$ th excited state level, g_A is the acceptor degeneracy factor of 4, and g_r is the $(1-1)$ th excited state degeneracy factor, which is expressed as r^2 . ΔE_r is described as¹⁹

$$\Delta E_r = \frac{q^4 m_h^*}{8h^2 \epsilon_0^2 \epsilon_s^2 r^2}, \quad (5)$$

and an ensemble average of the ground and excited state levels of acceptor $\overline{E_{\text{ex},n}(T)}$ is given by¹⁶⁻¹⁸

$$\overline{E_{\text{ex},n}(T)} = \frac{\sum_{r=2}^n (\Delta E_A - \Delta E_r) g_r \exp\left(-\frac{\Delta E_A - \Delta E_r}{k_B T}\right)}{1 + \sum_{r=2}^n g_r \exp\left(-\frac{\Delta E_A - \Delta E_r}{k_B T}\right)}, \quad (6)$$

where m_h^* is the hole effective mass for 4H-SiC, ϵ_0 is the vacuum permittivity, and ϵ_s is the static dielectric constant for 4H-SiC. Here, we used $\epsilon_s = (\epsilon_{\text{s||}} \epsilon_{\text{s\perp}}^2)^{1/3} = 9.78$, where $\epsilon_{\text{s||}} = 10.03$ and $\epsilon_{\text{s\perp}} = 9.66$ were taken from the value given by Patrick and Choyke,²⁰ and assumed $m_h^*/m_0 = 1$ for simplicity in the calculations of ΔE_r . The excited states were consid-

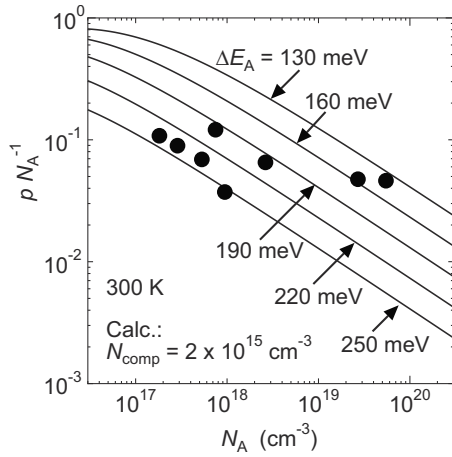


FIG. 3. The acceptor ionization ratio p/N_A as a function of the acceptor concentration at 300 K. The filled circles and solid curves indicate the experimental data and calculated results from the neutrality equation assuming the acceptor activation energies of 130, 160, 190, 220, and 250 meV, respectively.

ered up to sixth ($n=7$), which is sufficient for p -type SiC.¹⁸

In Fig. 2, the numerical results are plotted as solid lines, and the evaluated acceptor concentrations are also shown. On the other hand, the compensation ratio in our samples is so low that we could not define N_{comp} . Therefore we assumed $N_{\text{comp}}=0$ in the numerical results shown in Fig. 2. In spite of the assumption, they are well fitted to the experimental data in the temperature range from 200 to 500 K.

B. Ionization ratio and ionization energy of acceptors

Figure 3 shows the acceptor ionization ratio p/N_A as a function of the acceptor concentration at 300 K. Experimental data are denoted by filled circles. The solid curves indicate the results of the calculation from Eq. (2) assuming the Al acceptor ionization energy ΔE_A of 130, 160, 190, 220, and 250 meV with a constant compensation density N_{comp} of $2 \times 10^{15} \text{ cm}^{-3}$, which is the typical concentration of nitrogen donors in the undoped 4H-SiC samples grown under the present C/Si ratio by the CVD reactor employed in this study. The typical concentrations of deep traps in Al-doped epilayers are in the 10^{12} – 10^{13} cm^{-3} range,²¹ which is well below the nitrogen concentration. As well known, the ionization ratio is as low as 0.05–0.1, that is, the most part of the doped Al acceptors are as neutral impurities. As the acceptor concentration increases, the ionization ratio decreases because the Fermi level moves toward the valence band maximum E_V , and the neutral impurity concentration relatively increases. The decrease in ionization ratio is smaller than the calculated results assuming the same ionization energy, especially in the acceptor concentration higher than $2 \times 10^{18} \text{ cm}^{-3}$. This result arises from the reduced ionization energy of acceptors in heavily doped samples.

By fitting Eq. (2) to the experimental data, ΔE_A at each doping concentration can be determined. Figure 4 shows the ionization energy of the Al acceptors in 4H-SiC as a function of the acceptor concentration. The present data are similar to experimental values reported by Ivanov *et al.*,²² Matsuura *et al.*,²³ and Pernot *et al.*²⁴ The result experimentally obtained

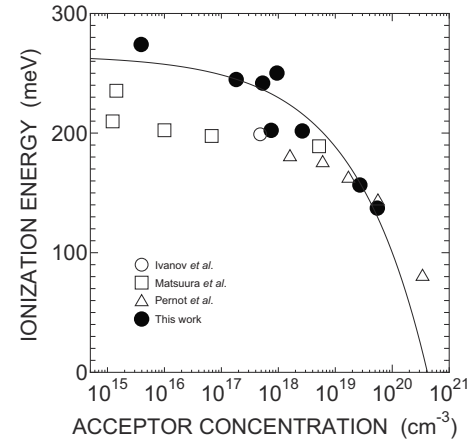


FIG. 4. Ionization energy of the acceptors in 4H-SiC as a function of the acceptor concentration. Experimental values of Ivanov *et al.* (Ref. 22), Matsuura *et al.* (Ref. 23), and Pernot *et al.* (Ref. 24) are also shown. The solid curve represents the empirical expression with $E_0=265 \text{ meV}$ and $\alpha=3.6 \times 10^{-5} \text{ meV cm}$.

for Al acceptors in 6H-SiC (Ref. 25) is also similar to the data shown in the figure. In general, it is known that the ionization energy depends strongly on the doping level. Several mechanisms describing the reduction in the ionization energy of impurities have been theoretically considered.²⁶ In a simple model, the reduction of the ionization energy is assumed to be inversely proportional to the average distance between the Al acceptors. This simple relation can be represented by the following expression:^{26–28}

$$\Delta E_A = \Delta E_0 - \alpha N_A^{1/3}, \quad (7)$$

where ΔE_0 is the ionization energy for infinite dilution and α is a proportion constant. The values of $\Delta E_0=265 \text{ meV}$ and $\alpha=3.6 \times 10^{-5} \text{ meV cm}$ were determined by fitting to our data. The dependence calculated using these values is plotted as a solid line in Fig. 4.

C. Numerical calculations of temperature dependence of Hall mobility

To determine which scattering mechanism determines the mobility in Al-doped 4H-SiC, we calculated mobilities limited by specific scattering mechanisms. In our calculations, five scattering mechanisms have been considered: ionized impurity (ii) scattering, neutral impurity (ni) scattering, acoustic phonon (ac) scattering, polar optical-phonon (pop) scattering, and nonpolar optical-phonon (npo) scattering. For convenience, a detailed description of the specific relaxation time is given in Appendix.

The drift mobility for hole perpendicular to the c axis is obtained by

$$\mu = \frac{q \langle \tau \rangle}{m_{h\perp}^*}, \quad (8)$$

where $m_{h\perp}^* = 0.66m_0$ is the hole effective mass in the basal plane,²⁹ $\langle \tau \rangle$ is the average total relaxation time, it can be written for a nondegenerate semiconductor,

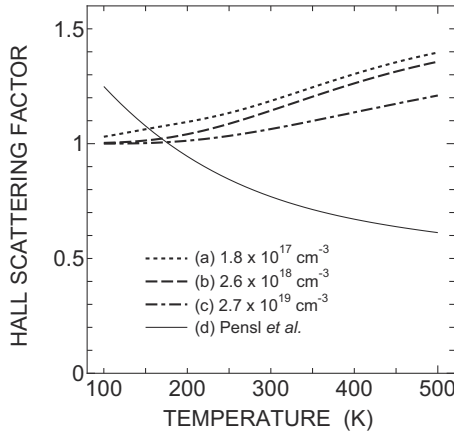


FIG. 5. Hall scattering factor for holes in Al-doped 4H-SiC with the acceptor concentrations of (a) 1.8×10^{17} , (b) 2.6×10^{18} , and (c) 2.7×10^{19} cm^{-3} as a function of the temperature calculated with Eq. (12). The solid curve shows the experimental results of the Hall scattering factor obtained by Pensl *et al.* (Ref. 30).

$$\langle \tau \rangle = \frac{\int_0^{\infty} \varepsilon^{3/2} \tau_{\text{total}}(\varepsilon) \exp\left(-\frac{\varepsilon}{k_B T}\right) d\varepsilon}{\int_0^{\infty} \varepsilon^{3/2} \exp\left(-\frac{\varepsilon}{k_B T}\right) d\varepsilon}, \quad (9)$$

where $\tau_{\text{total}}(\varepsilon)$ is the hole momentum relaxation time for a hole having the kinetic energy ε . $\tau_{\text{total}}(\varepsilon)$ is given by

$$\frac{1}{\tau_{\text{total}}(\varepsilon)} = \frac{1}{\tau_{\text{ii}}(\varepsilon)} + \frac{1}{\tau_{\text{ni}}(\varepsilon)} + \frac{1}{\tau_{\text{ac}}(\varepsilon)} + \frac{1}{\tau_{\text{pop}}(\varepsilon)} + \frac{1}{\tau_{\text{npo}}(\varepsilon)}, \quad (10)$$

where $\tau_{\text{ii}}(\varepsilon)$, $\tau_{\text{ni}}(\varepsilon)$, $\tau_{\text{ac}}(\varepsilon)$, $\tau_{\text{pop}}(\varepsilon)$, and $\tau_{\text{npo}}(\varepsilon)$ are the relaxation times for a hole having the kinetic energy ε due to ionized impurity scattering, neutral impurity scattering, acoustic phonon scattering, polar optical-phonon scattering, and nonpolar optical-phonon scattering, respectively.

The Hall mobility can be calculated by

$$\mu_H = r_H \mu. \quad (11)$$

The magnitude of Hall scattering factor depends on the scattering mechanisms. It can be calculated with the expression under a low-magnetic field condition,

$$r_H = \frac{\langle \tau^2 \rangle}{\langle \tau \rangle^2}, \quad (12)$$

where $\langle \tau^2 \rangle$ is the average total square relaxation time given by

$$\langle \tau^2 \rangle = \frac{\int_0^{\infty} \varepsilon^{3/2} \tau_{\text{total}}^2(\varepsilon) \exp\left(-\frac{\varepsilon}{k_B T}\right) d\varepsilon}{\int_0^{\infty} \varepsilon^{3/2} \exp\left(-\frac{\varepsilon}{k_B T}\right) d\varepsilon}. \quad (13)$$

Figure 5 shows the Hall scattering factor r_{calc} as a function of the temperature calculated for holes in Al-doped 4H-SiC using Eq. (12) with the acceptor concentrations of (a) 1.8×10^{17} , (b) 2.6×10^{18} , and (c) 2.7×10^{19} cm^{-3} . The experimental temperature dependence of the Hall scattering

factor r_{exp} was also shown in Fig. 5, which was determined by Pensl *et al.*³⁰ from comparing the experimental hole concentration measured by Hall effect with the hole concentration calculated based on the neutrality equation and the defect parameters determined by secondary ion mass spectrometry and capacitance-voltage technique. The temperature dependence of r_{calc} is slightly different for different acceptor concentrations because the dominant scattering factors are changed. In the acceptor concentration range lower than 10^{18} cm^{-3} , the dominant scattering factor is the lattice scattering as shown in Fig. 6(a), and the Hall scattering factor is insensitive to the acceptor concentration. It is noted that r_{exp} was tested in the range from 10^{15} to 10^{18} cm^{-3} using Al-doped 4H-SiC epilayer samples by Schmid *et al.*,⁸ and they concluded that the Hall scattering factor in weakly compensated *p*-type 4H-SiC does not critically depend on the Al acceptor concentration. This result is consistent with our calculations. However, r_{exp} and r_{calc} show the opposite dependence on temperature and r_{exp} is significantly lower than that of r_{calc} in the temperature range higher than 200 K. The difference of the Hall scattering factor obtained by calculation and experiment in *p*-type material has been also shown in GaAs by Look *et al.*³¹ They have concluded that the difference was caused by either the hole scattering theories inadequately describe Hall-effect data or the experimental errors of acceptor concentration measured by electrochemical capacitance-voltage measurements. The compensation ratio may also play an important role especially in the low temperature range. The effects of the compensation ratio on the Hall scattering factor and the hole mobility are still under study. In the acceptor concentration range higher than 10^{18} cm^{-3} , on the other hand, the dominant scattering factor is changed to the neutral impurity scattering as shown in Fig. 6, and the Hall scattering factor close to unity. In this work, we use the calculated Hall scattering factor in the calculation of hole Hall mobility.

Figure 6 shows the experimental Hall mobility for the samples with the acceptor concentrations of (a) 1.8×10^{17} , (b) 2.6×10^{18} , and (c) 2.7×10^{19} cm^{-3} as a function of temperature. The solid curves show the calculated Hall mobility for holes. The contributions of various scattering mechanisms to the total hole Hall mobility are also shown by broken lines. The concentration of ionized impurities $N_{\text{ii}}(T)$ and neutral impurities $N_{\text{ni}}(T)$ are given by $N_{\text{ii}}(T) = 2N_{\text{comp}} + p(T)$ and $N_{\text{ni}}(T) = N_A - N_{\text{comp}} - p(T)$, respectively. Thus, the mobilities determined by the neutral impurity scattering and ionized impurity scattering are strongly dependent on the acceptor concentration.

For the sample with the low acceptor concentration [Fig. 6(a)], the mobility decreases with increasing temperature according to the $T^{-1.5}$ dependence below 200 K, and this dependence can be explained by the dominance of acoustic phonon scattering. In the temperature range higher than approximately 250 K, the mobility decreases with increasing temperature according to the $T^{-2.6}$ dependence. This rapid decrease in the hole mobility may be attributed to the increased scattering rate for nonpolar optical-phonon scattering. In the very low temperature range (~ 100 K), the mobility component due to the neutral impurity scattering also

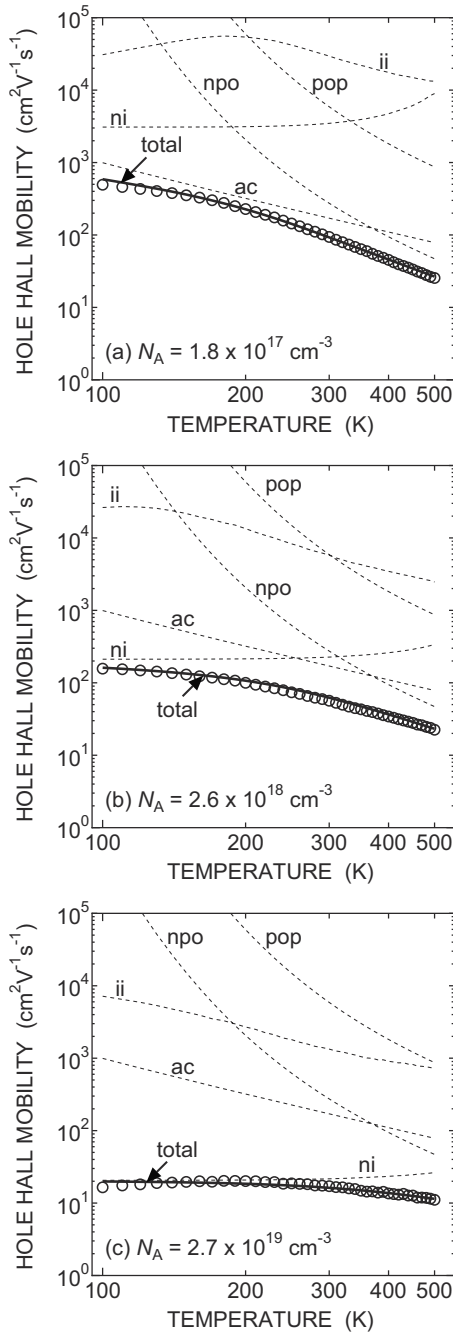


FIG. 6. Experimental hole Hall mobility for the samples with the acceptor concentrations of (a) 1.8×10^{17} , (b) 2.6×10^{18} , and (c) 2.7×10^{19} cm^{-3} as a function of the temperature. The broken curves show the individual theoretical contribution of various scattering mechanisms to limit the Hall mobility. The scattering mechanisms are ionized impurities (ii), neutral impurity (ni), acoustic phonon (ac), polar optical phonon (pop), and nonpolar optical phonon (npo). The solid curves show the total Hall mobility considering all the scattering mechanisms.

affects the hole mobility, although the influence is rather small. It should be noted that the hole mobility is not governed by the mobility component due to the ionized impurity scattering even at low temperature because of the large ionization energy of Al acceptor and the low compensation level. For the sample with an acceptor concentration of 2.6×10^{18} cm^{-3} [Fig. 6(b)], the neutral impurity scattering is the most dominant limiting factor of the hole mobility in the temperature range lower than 250 K. On the other hand, in

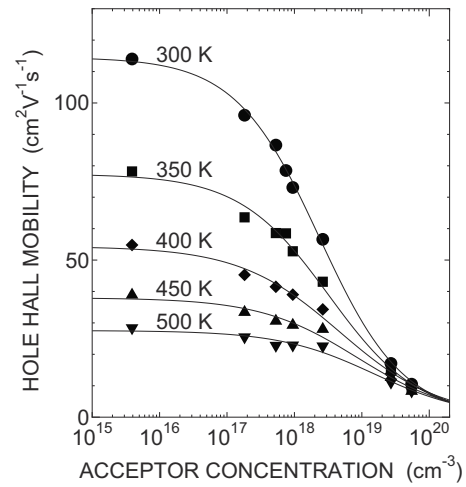


FIG. 7. Experimental hole Hall mobility as a function of acceptor concentration at the temperature stepped from 300 to 500 K in 50 K increments. The solid curves depict the fitting results to an empirical Caughey–Thomas model assuming the minimum mobility $\mu_{\min}=0$ $\text{cm}^2/\text{V s}$.

the higher temperature range, the hole mobility is more limited by phonon scattering. For the sample with the higher acceptor concentration, the measured mobility shows the feature of neutral impurity scattering, which is insensitive to temperature, as shown in Fig. 6(c). The neutral impurity scattering dominates in all the temperature range from 100 to 500 K in this sample. Because the ionization energy is larger than 100 meV, as shown in Fig. 4, the ionization ratio of Al acceptors in 4H-SiC is less than 20% even at 500 K. As a result, most of the acceptors work as neutral impurities, and the neutral impurity scattering, instead of ionized impurity scattering, is an important limiting factor for the hole mobility in the heavily doped 4H-SiC.

D. Parameters for mobility model

The results of our calculations illustrate the importance of neutral impurity scattering in the determination of hole mobility and are in good agreement with mobility values experimentally measured in wide ranges of temperature and acceptor concentration. However, the computational technique, based on the solution of the Boltzmann transport equation, is not convenient for use in device analyses. The hole mobility in *p*-type 4H-SiC has been evaluated by using a Caughey–Thomas empirical model,^{6,32} which is expressed as

$$\mu(T, N_{\text{imp}}) = \mu_{\min} + \frac{\mu_{\max}(T) - \mu_{\min}}{1 + \left[\frac{N_{\text{imp}}}{N_{\text{ref}}(T)} \right]^{\gamma(T)}}, \quad (14)$$

where μ_{\min} is the minimum mobility, $\mu_{\max}(T)$ the maximum mobility, N_{imp} the impurity concentration which affects the mobility, $N_{\text{ref}}(T)$ the reference concentration, and $\gamma(T)$ the fitting parameter. Figure 7 shows the hole Hall mobility as a function of acceptor concentration at the temperatures stepped from 300 to 500 K in 50 K increments. The solid curves depict the fitting results, assuming $\mu_{\min}=0$ $\text{cm}^2/\text{V s}$. The variations of temperature dependent parameters in Caughey–Thomas model for Al-doped 4H-SiC are shown in

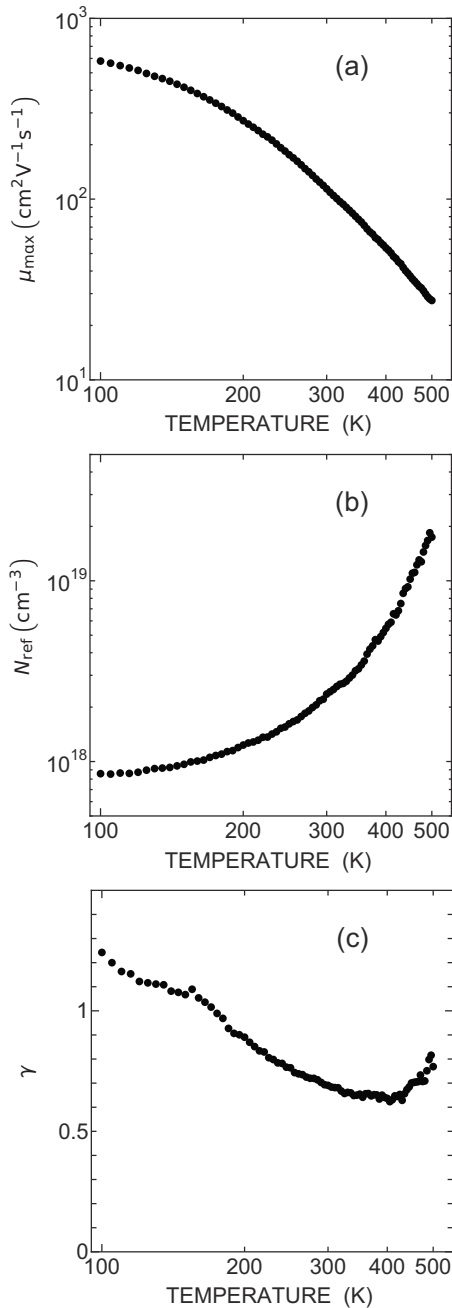


FIG. 8. Caughey-Thomas parameters (a) $\mu_{\max}(T)$, (b) $N_{\text{ref}}(T)$, and (c) $\gamma(T)$ in Al-doped 4H-SiC as a function of temperature.

Fig. 8. These values are obtained by fitting to our data at each temperature. By using these parameters, the hole mobility at any acceptor concentrations in the wide temperature range can be predicted, which is useful for device simulation. The present parameters may be valid for Al-doped 4H-SiC with a low degree of compensation, and a slightly different set of parameters may be required for highly compensated materials such as the Al-implanted layers. The influence of compensation is under investigation. The physical meanings of Eq. (14) can be considered as follows.³³

- (1) N_{imp} usually denotes the total concentration of ionized impurities.^{6,34} In the present case, however, the mobility is mainly reduced by neutral impurity scattering as mentioned in Fig. 6, especially for heavily doped samples.

Because of the small ionization ratio of acceptors, we consider that the neutral impurity concentration is approximately equal to the acceptor concentration. Thus, we assumed $N_{\text{imp}} \approx N_A$.

- (2) At very low acceptor concentration with low compensation, mobility saturates at $\mu_{\max}(T)$, which is the lattice-limited mobility.
- (3) At very high doping concentration, mobility saturates at μ_{\min} , which is temperature independent for conventional semiconductors such as Si and GaAs, because degenerate semiconductors show an almost temperature-insensitive mobility. In the case of *p*-type 4H-SiC, however, the temperature-insensitive neutral impurity scattering limits the mobility in the acceptor concentration range up to $5.5 \times 10^{19} \text{ cm}^{-3}$. The mobility is proportional to the inverse of neutral impurity concentration. Therefore, it may be reasonable to assume $\mu_{\min} = 0 \text{ cm}^2/\text{V s}$.
- (4) At the acceptor concentration around $N_{\text{ref}}(T)$, the contributions of lattice scattering and that of impurity scattering to the mobility are almost the same. Since the lattice scattering mechanisms dominate at higher temperatures, the contribution of neutral impurity scattering is started at higher acceptor concentrations, at high temperature, as shown in Fig. 6. Therefore, $N_{\text{ref}}(T)$ increases with increasing temperature.
- (5) $\gamma(T)$ is the temperature dependent parameter corresponding to the reduction of mobility with increasing acceptor concentration around $N_{\text{ref}}(T)$, which is limited by impurity scattering. The value of $\gamma(T)$ at low temperature below 150 K is approximately unity. In the temperature range from 150 to 500 K, $\gamma(T)$ decreases and reaches about 0.5–0.6. The decrease in $\gamma(T)$ may be attributed to increasing concentration of the ionized impurity and decreasing that of neutral impurity with increasing temperature. As a result, the contribution of the neutral impurity scattering decreases.

IV. CONCLUSIONS

We have investigated the electrical properties of Al-doped 4H-SiC epilayers grown on semi-insulating substrates in the acceptor concentration range from 3×10^{15} to $5.5 \times 10^{19} \text{ cm}^{-3}$ using Hall-effect measurements. The most portion of the doped Al acceptors works as neutral impurities due to the large ionization energy. By comparing theoretical and experimental values of temperature dependent hole Hall mobility, the dominant scattering mechanism has been discussed. The neutral impurity scattering becomes a significant factor when the acceptor concentration is higher than 10^{18} cm^{-3} , especially at temperature lower than 300 K. In heavily doped samples ($\geq 10^{19} \text{ cm}^{-3}$), the hole mobility is limited by the neutral impurity scattering even at higher temperature. A Caughey-Thomas model was employed for analyzing the low-field mobility as a function of Al acceptor concentration and temperature. An appropriate parameter set for Al-doped 4H-SiC with low compensation was obtained by fitting to the Hall mobility data.

APPENDIX: SCATTERING MECHANISMS

1. IONIZED IMPURITY SCATTERING

The scattering by ionized impurities is calculated using the Brooks–Herring model,³⁵ which uses the screened Coulomb interaction for the scattering potential and treats the scattering probability in the first Born approximation. To take into account the p -like wave functions, the relaxation time in the valence band is multiplied by a factor of $3/2$, as discussed in Ref. 36. The relaxation time is

$$\frac{1}{\tau_{ii}} = \frac{2}{3} \frac{q^4 N_{ii} L(2k\lambda_D)}{16\pi(2m_h^*)^{1/2} \epsilon_s^2 \epsilon_0^2} \epsilon^{-3/2}, \quad (\text{A1})$$

where ϵ_s is the static dielectric constant, ϵ_0 is the vacuum permittivity, and $L(2k\lambda_D)$ is given by

$$L(2k\lambda_D) = \ln(1 + 4k^2\lambda_D^2) - \frac{4k^2\lambda_D^2}{4k^2\lambda_D^2 + 1}, \quad (\text{A2})$$

where k is the electron wave vector, λ_D the Debye screening length given by

$$\lambda_D = \sqrt{\frac{\epsilon_s \epsilon_0 k_B T}{q^2 p'}}, \quad (\text{A3})$$

where

$$p' = p + \frac{(N_A - N_D - p)(N_D + p)}{N_A} \quad (\text{A4})$$

is the screening hole concentration surrounding the ionized impurity, in which N_D is the donor concentration. Assuming spherical parabolic bands, we used $k = (2m_h^* \epsilon / \hbar^2)^{1/2}$ in the calculations, where m_h^* is the effective mass of hole, which was estimated to be $0.5m_0$ by fitting to the experimental data.

2. NEUTRAL IMPURITY SCATTERING

The scattering due to the neutral impurity is an important source of resistance at very low temperatures in a conventional semiconductor because shallow-level impurities become neutral only at very low temperatures. In Al-doped 4H-SiC, however, most of the acceptors are not ionized even at 500 K because of the large ionization energy of Al acceptor. Therefore the neutral impurity is a significant scattering source at the measured temperatures. The relaxation time for the neutral impurity scattering was calculated by making use of Erginsoy's equation,^{37,38}

$$\frac{1}{\tau_{ni}} = \frac{10\epsilon_s \epsilon_0 N_{ni} \hbar^3}{\pi^2 m_h^{*2} q^2}, \quad (\text{A5})$$

where $N_{ni} = N_A - N_{\text{comp}} - p$ is the concentration of neutral impurities and \hbar is the Planck constant.

3. ACOUSTIC PHONON SCATTERING

The scattering by acoustic phonons is the most important scattering source in intrinsic or lightly doped semiconductors at room temperature or higher temperatures. The relaxation time is given by³⁹

$$\frac{1}{\tau_{ac}} = \frac{\sqrt{2} m_{\text{dh}}^{*3/2} k_B T E_{v1} \epsilon^{1/2}}{\pi \hbar^4 \rho v_{\parallel}}, \quad (\text{A6})$$

where ρ is the mass density of the atom, v_{\parallel} the velocity of longitudinal acoustic phonons, and E_{v1} the acoustic deformation potential. We take $\rho = 3211 \text{ kg m}^{-3}$ as determined by Gomes for 6H-SiC (Ref. 40) and $v_{\parallel} = 13730 \text{ m s}^{-1}$ as determined by Karmann *et al.*⁴¹ for the sound velocity along the hexagonal axis. E_{v1} was estimated to be $E_{v1} = 9.5 \text{ eV}$ by fitting to the experimental data in the lowest acceptor concentration sample.

4. POLAR OPTICAL-PHONON SCATTERING

The relaxation time for the polar optical phonon scattering, derived by Callen,⁴² is given by

$$\begin{aligned} \frac{1}{\tau_{\text{pop}}} = \frac{1}{24\pi\epsilon_p \hbar (2\epsilon/m_{\text{dh}}^*)^{1/2}} & \left\{ n(\omega_{\text{op}}) \left(1 + \frac{\hbar\omega_{\text{op}}}{\epsilon} \right)^{1/2} + H(\epsilon) \right. \\ & - \hbar\omega_{\text{op}} [n(\omega_{\text{op}}) + 1] \left(1 - \frac{\hbar\omega_{\text{op}}}{\epsilon} \right)^{1/2} + \frac{\hbar\omega_{\text{op}}}{\epsilon} [\\ & - n(\omega_{\text{op}})] \sinh^{-1} \left(\frac{\epsilon}{\hbar\omega_{\text{op}}} \right)^{1/2} + H(\epsilon) \\ & - \hbar\omega_{\text{op}} \frac{\hbar\omega_{\text{op}}}{\epsilon} [n(\omega_{\text{op}}) + 1] \sinh^{-1} \left\{ \left(\frac{\epsilon}{\hbar\omega_{\text{op}}} \right. \right. \\ & \left. \left. - 1 \right)^{1/2} \right\} \left. \right\}, \quad (\text{A7}) \end{aligned}$$

where $\hbar\omega_{\text{op}}$ denotes the polar optical-phonon energy and $H(\epsilon - \hbar\omega_{\text{op}})$ is the Heaviside step function. The term ϵ_p is determined through the following relationship: $1/\epsilon_p = 1/(\epsilon_{\infty}\epsilon_0) - 1/(\epsilon_s\epsilon_0)$, where ϵ_{∞} and ϵ_s represent the high-frequency and static relative dielectric constants, respectively, ϵ_0 denoting the dielectric constant in vacuum. $n(\omega_{\text{op}})$ represents the phonon occupation factor of the polar optical phonons of energy $\hbar\omega_{\text{op}}$, that is given by the Bose distribution $n(\omega_{\text{op}}) = [\exp\{\hbar\omega_{\text{op}}/(k_B T)\} - 1]^{-1}$. Since the multiphonon scattering is not expected to play a significant role, the term $n(\omega_{\text{op}}) + 1$ contributes only when it is energetically possible (i.e., $\epsilon \geq \hbar\omega_{\text{op}}$). The factor of $1/2$ arises from the p -like symmetry of the wave functions.⁴³ We take $\hbar\omega_{\text{op}} = 120 \text{ meV}$ (Ref. 44) for the polar optical-phonon energy at small values of the phonon wave vector. For the dielectric constant ϵ_{∞} , we took $\epsilon_{\infty} = (\epsilon_{\infty\parallel}\epsilon_{\infty\perp})^{1/3} = 6.58$, where $\epsilon_{\infty\parallel} = 6.70$ and $\epsilon_{\infty\perp} = 6.52$ were taken from the values given by Patrick and Choyke.²⁰

5. NONPOLAR OPTICAL-PHONON SCATTERING

The relaxation time for the nonpolar optical-phonon scattering valid for p -like wave functions is given by^{37,45,46}

$$\begin{aligned} \frac{1}{\tau_{\text{npo}}} = \frac{D_0^2 m_{\text{dh}}^{*3/2}}{\sqrt{2}\pi\rho\hbar^3\omega_0} & \times \{n(\omega_0)(\epsilon + \hbar\omega_0)^{1/2} + H(\epsilon - \hbar\omega_0) \\ & \times [n(\omega_0) + 1](\epsilon - \hbar\omega_0)^{1/2}\}, \quad (\text{A8}) \end{aligned}$$

where $n(\omega_0) = [\exp\{\hbar\omega_0/(k_B T)\} - 1]^{-1}$ is the phonon occupation factor and $H(\epsilon - \hbar\omega_0)$ is the Heaviside step function. D_0

denotes the optical deformation potential. In the calculations, we use D_0 estimated to be $D_0=2.8 \times 10^{11}$ eV/m by fitting to the experimental data in the lowest acceptor concentration sample. The phonon emission terms $n(\omega_0)+1$ contribute only for $\varepsilon \geq \hbar\omega_0$. Since the difference between the frequencies of the longitudinal optical-phonon (ω_{LO}) and transverse optical-phonon (ω_{TO}) is not very large, it is a reasonable approximation to adopt a single frequency for the optical-phonon energy, we use a representative phonon energy $\hbar\omega_0 = 100$ meV. This phonon energy corresponds to an average energy of the optical-phonon modes at the Γ point of the Brillouin zone.⁴⁴

- ¹M. Bhatnagar and B. J. Baliga, *IEEE Trans. Electron Devices* **40**, 645 (1993).
- ²H. Matsunami and T. Kimoto, *Mater. Sci. Eng. R.* **20**, 125 (1997).
- ³J. Pernot, S. Contreras, J. Camassel, J. L. Robert, W. Zawadzki, E. Neyret, and L. D. Cioccio, *Appl. Phys. Lett.* **77**, 4359 (2000).
- ⁴H. Iwata and K. M. Itoh, *J. Appl. Phys.* **89**, 6228 (2001).
- ⁵J. Pernot, W. Zawadzki, S. Contreras, J. L. Robert, E. Neyret, and L. D. Cioccio, *J. Appl. Phys.* **90**, 1869 (2001).
- ⁶T. Hatakeyama, T. Watanabe, M. Kushibe, K. Kojima, S. Imai, T. Suzuki, T. Shinohe, T. Tanaka, and K. Arai, *Mater. Sci. Forum* **433–436**, 443 (2003).
- ⁷W. J. Schaffer, G. H. Negley, K. G. Irvine, and J. Palmour, *Mater. Res. Soc. Symp. Proc.* **339**, 595 (1994).
- ⁸F. Schmid, M. Krieger, M. Laube, G. Pensl, and G. Wagner, in *Silicon Carbide: Recent Major Advances*, edited by J. Choyke, H. Matsunami, and G. Pensl (Springer-Verlag, Berlin Heidelberg, New York, 2004), pp. 517–536.
- ⁹M. Ikeda, H. Matsunami, and T. Tanaka, *Phys. Rev. B* **22**, 2842 (1980).
- ¹⁰N. I. Kuznetsov and A. S. Zubrilov, *Mater. Sci. Eng., B* **29**, 181 (1995).
- ¹¹T. Troffer, C. Hüßler, G. Pensl, K. Hölzlein, H. Mitlehner, and J. Völkl, *Inst. Phys. Conf. Ser.* **142**, 281 (1996).
- ¹²T. Stiasny and R. Helbig, *Inst. Phys. Conf. Ser.* **142**, 389 (1996).
- ¹³T. Kimoto, A. Itoh, and H. Matsunami, *Phys. Status Solidi B* **202**, 247 (1997).
- ¹⁴G. Wellenhofer and U. Rössler, *Phys. Status Solidi B* **202**, 107 (1997).
- ¹⁵J. S. Blakemore, *Semiconductor Statistics* (Dover, New York, 1987) pp. 117–176.
- ¹⁶H. Matsuura, *New J. Phys.* **4**, 12.1 (2002) [<http://www.njp.org/>].
- ¹⁷H. Matsuura, K. Sugiyama, K. Nishikawa, T. Nagata, and N. Fukunaga, *J. Appl. Phys.* **94**, 2234 (2003).
- ¹⁸H. Matsuura, *J. Appl. Phys.* **95**, 4213 (2004).
- ¹⁹P. Y. Yu and M. Cardona, *Fundamentals of Semiconductors: Physics and Materials Properties*, 2nd ed. (Springer, Berlin, 1999), p. 156.
- ²⁰L. Patrick and W. J. Choyke, *Phys. Rev. B* **2**, 2255 (1970).
- ²¹K. Danno and T. Kimoto, *J. Appl. Phys.* **101**, 103704 (2007).
- ²²I. G. Ivanov, B. Magnusson, and E. Janzén, *Phys. Rev. B* **67**, 165211 (2003).
- ²³H. Matsuura, M. Komeda, S. Kagamihara, H. Iwata, R. Ishihara, T. Hatakeyama, T. Watanabe, K. Kojima, T. Shinohe, and K. Arai, *J. Appl. Phys.* **96**, 2708 (2004).
- ²⁴J. Pernot, S. Contreras, and J. Camassel, *J. Appl. Phys.* **98**, 023706 (2005).
- ²⁵A. Schöner, N. Nordell, K. Rottner, R. Helbig, and G. Pensl, *Inst. Phys. Conf. Ser.* **142**, 493 (1996).
- ²⁶G. I. Pearson and J. Bardeen, *Phys. Rev.* **75**, 865 (1949).
- ²⁷P. P. Debye and E. M. Conwell, *Phys. Rev.* **93**, 693 (1954).
- ²⁸C. Y. Chang, M. C. Wu, Y. K. Su, C. Y. Nee, and K. Y. Cheng, *J. Appl. Phys.* **58**, 3907 (1985).
- ²⁹N. T. Son, P. N. Hai, W. M. Chen, C. Hallin, B. Monemar, and E. Janzén, *Phys. Rev. B* **61**, R10544 (2000).
- ³⁰G. Pensl, F. Schmid, F. Ciobanu, M. Laube, S. A. Reshanov, N. Schulze, K. Semmelroth, H. Nagasawa, A. Schöner, and G. Wagner, *Mater. Sci. Forum* **433–436**, 365 (2003).
- ³¹D. C. Look, C. E. Stutz, J. R. Sizelove, and K. R. Evans, *J. Appl. Phys.* **80**, 1913 (1996).
- ³²D. M. Caughey and R. E. Thomas, *Proc. IEEE* **55**, 2192 (1967).
- ³³M. Sotoodeh, A. H. Khalid, and A. A. Rezazadeh, *J. Appl. Phys.* **87**, 2890 (2000).
- ³⁴Y. Negoro, T. Kimoto, and H. Matsunami, *J. Appl. Phys.* **96**, 4916 (2004).
- ³⁵H. Brooks, *Advances in Electronics and Electron Physics* (Academic, New York, 1955), Vol. 7, pp. 85–182.
- ³⁶J. D. Wiley, *Semiconductors and Semimetals* (Academic, New York, 1975), Vol. 10.
- ³⁷B. K. Ridley, *Quantum Processes in Semiconductors*, 4th ed. (Clarendon, Oxford, 1999).
- ³⁸C. Erginsoy, *Phys. Rev.* **79**, 1013 (1950).
- ³⁹M. Costato, G. Gagliani, C. Jacoboni, and L. Reggiani, *J. Phys. Chem. Solids* **35**, 1605 (1974).
- ⁴⁰A. H. G. de Mesquita, *Acta Crystallogr.* **23**, 610 (1967).
- ⁴¹S. Karmann, R. Helbig, and R. A. Stein, *J. Appl. Phys.* **66**, 3922 (1989).
- ⁴²H. B. Callen, *Phys. Rev.* **76**, 1394 (1946).
- ⁴³J. D. Wiley, *Phys. Rev. B* **4**, 2485 (1971).
- ⁴⁴D. W. Feldman, J. J. H. Parker, W. J. Choyke, and L. Patrick, *Phys. Rev.* **173**, 787 (1968).
- ⁴⁵D. C. Look, *Electrical Characterization of GaAs Materials and Devices* (Wiley, New York, 1989).
- ⁴⁶E. M. Conwell and M. O. Vassell, *Phys. Rev.* **166**, 797 (1968).